

Resonant X-ray Scattering: A Tool for Structure Elucidation in Liquid Crystals

Helen F. Gleeson^{*[a]} and Linda S. Hirst^[b]

The use of resonant X-ray scattering to determine structures in liquid crystal systems is surveyed. This powerful experimental technique utilises “forbidden reflections” to determine the subtle differences in interlayer orientation that differentiate several smectic systems. The technique relies on the materials containing an atom to which the X-ray energy can be tuned, usually sulphur or selenium. Experiments are often carried out on free-standing films that provide a highly monodomain structure that allows high-resolution measurements to be made, and, hence, structural

details to be determined. Alternatively, resonant scattering has been demonstrated for materials contained in glass devices that permit the application of electric fields to the system, in a manner analogous to that used in liquid crystal devices. The resonant scattering technique provides unequivocal descriptions of the packing in smectic systems, and the way in which the packing is distorted in electric fields. This Minireview describes the principles behind resonant X-ray scattering, its application to liquid crystals and some of the potential for the future.

Introduction

X-ray scattering has long been recognised as an important tool in the study of structure in soft condensed matter systems where the molecular length is often the unit that defines the structural length scale. Liquid crystals (LCs) form a significant subclass of soft condensed matter systems and can be broadly described as ordered fluids formed from geometrically anisotropic molecules. There are many ways in which this concept can be realised, and as a result there is a rich array of liquid crystal phases.^[1] The class of liquid crystals of most interest in the context of this Minireview are the smectic phases. These are formed from rodlike molecules and are characterised by a combination of orientational order (defined by a *director*, the average direction in which the molecules point) and a degree of positional order (a density wave, or layers, formed within the structure). The smectic layer spacing is typically of the order of a molecular length and X-ray scattering has been particularly valuable in determining the structures of the various phases that are possible. There are some excellent reviews of X-ray studies of liquid crystals including the chapter by Seddon in ref. [1] and articles by Pershan,^[2] Kumar,^[3] and Clegg.^[4]

A major limitation of “conventional” X-ray scattering is that it is not sensitive to the local environment of a molecule, and so cannot distinguish between smectic liquid crystal phases that differ with respect to the orientation (but not packing) of the molecules in successive layers. An example is shown in Figure 1, which shows four similar smectic liquid crystal phases that are described in detail later in this article. A different scattering situation occurs in resonant scattering when the energy of the X-ray is tuned to the absorption edge of an atom in the structure. Then, the scattering process can involve the promotion of core electrons to states above the Fermi level, which are in turn influenced by chemical bonding and the local environment of the molecule. As a consequence, the atomic scattering factor becomes a tensor allowing “forbidden” reflections

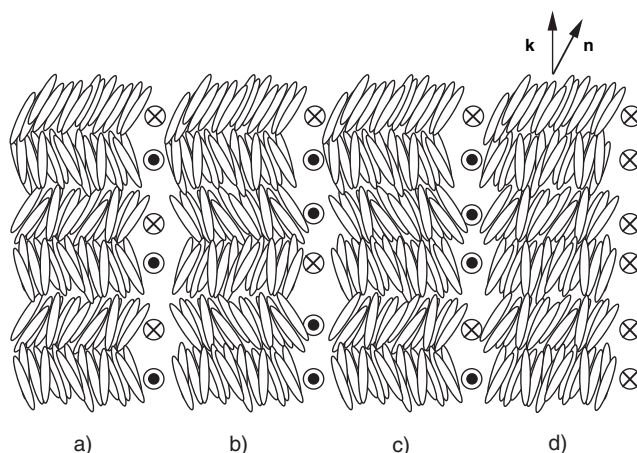


Figure 1. A cartoon showing four tilted smectic phases with subtle differences in their interlayer structures: a) an anticlinic phase (SmC_A^*); b) and c) intermediate (ferrielectric) phases; d) a synclinic phase (SmC^*). The director and layer normal are denoted by the unit vectors \mathbf{n} and \mathbf{k} , respectively. Each of these phases gives an identical X-ray scattering signal in conventional small-angle scattering experiments, but the different local structures give rise to characteristic “forbidden” reflections in resonant scattering experiments. The helicoidal superstructure associated with these chiral smectic structures is not shown as the helical pitch typically repeats over several hundred layers. The fact that these phases can exhibit ferroelectricity, ferrielectricity, and antiferroelectricity is indicated by the fact that circles represent the layer dipoles, pointing into (\otimes) and out of (\odot) the page.

[a] Prof. H. F. Gleeson
School of Physics and Astronomy
The University of Manchester, Manchester M13 9PL (UK)
Fax: (+44) 161-275-4056
E-mail: helen.gleeson@manchester.ac.uk

[b] Dr. L. S. Hirst
School of Physics
Florida State University, Tallahassee, FL 32306-4350 (USA)

to be observed that are also polarisation-dependant. Templeton and Templeton^[5] first recognised the opportunity that this presented for the study of materials as the forbidden reflections are a direct result of scattering from atoms that probe their local environment. A general theory of forbidden reflections was presented by Dmitrienko,^[6,7] with the first experimental observations made by Templeton and Templeton.^[8] The technique was not applied to liquid crystals until after the discovery of smectic systems with very subtle structural differences.

If the molecules that form a liquid crystal are chiral, the bulk phase can sometimes also be chiral in which case it is often characterised by a helicoidal superstructure.^[9] The inherent reduction in symmetry makes it possible for such liquid crystals to exhibit ferroelectricity^[10] and antiferroelectricity. These properties are most commonly observed in variations of the chiral smectic-C (SmC*) phase,^[11] some of which are shown in Figure 1. In the SmC* phases, the director, \mathbf{n} , is tilted by a temperature-dependant angle with respect to the layer normal, \mathbf{k} . The ferroelectricity of the synclinal SmC* phase is associated with the fact that dipoles, which for symmetry reasons must lie perpendicular to the layer normal and tilt plane, all lie in the same direction, producing a bulk dipole (spontaneous polarisation) in the phase. The anticlinical SmC* phase^[12] similarly exhibits antiferroelectricity, while the intermediate phases with three- or four-layer repeats shown could be ferrielectric.^[13,14] The discovery of these closely related liquid crystal phases in the early 1990s led to considerable debate about both the structure and the possible number of intermediate phases. It was only when resonant scattering experiments were applied to differentiate between the different possible structures that their actual structures were confirmed.^[15]

This Minireview summarises the theory of resonant scattering, describing where the forbidden reflections occur in liquid crystal systems and what information they can contain. The relevant experimental techniques are described in detail, showing the various types of resonant signal that can be obtained and analysed. There are some areas where resonant X-ray scattering has not yet been successfully applied and these are also described, indicating the promise of the technique for the future.

Theory of Forbidden Reflections in Liquid Crystals

Dmitrienko^[6] investigated the structure factors of forbidden reflections in several symmetries, showing that by carrying out X-ray scattering experiments at the absorption edge of a particular atom in the crystal structure, forbidden reflections could be observed. The predictions from crystallography were taken by Levelut and Pansu^[16] and adapted to the specific case of smectic liquid crystals. The resonant technique can probe periodicities in molecular orientation, in the case of smectic liquid crystals allowing the determination of the number of layers that make up specific structures. Further, consideration of the polarisation properties of the resonant scattered X-rays can distinguish between different orientational arrangements.

Both features are important in liquid crystals as they provide a method to examine some key theories that explain both the occurrence and structure of the intermediate phases directly; for example, during the 1990s, at least three distinct structures were proposed for the SmC* intermediate phases, including an Ising model, a clock model,^[17–19] and a model by Lorman.^[20] Features of the three different models are shown schematically in Figure 2. It can be seen from the figure why there is some

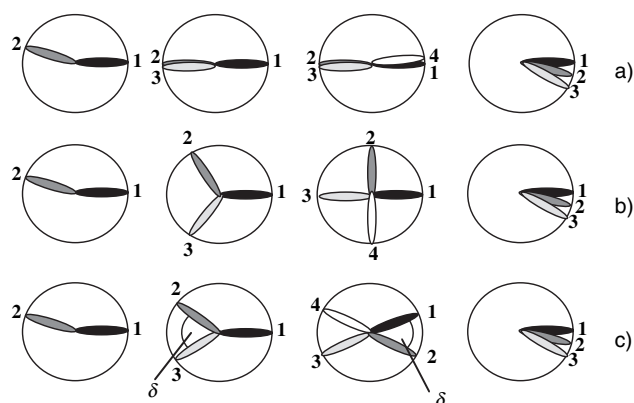


Figure 2. A cartoon of the different models of the intermediate phases, showing projections of the molecules as viewed from the direction of the layer normal. The SmC_A* phase is on the left and the SmC* on the right. Three different models of the three- and four-layer intermediate phases are demonstrated: a) the Ising model, where the structure is essentially two-dimensional with only the helicoidal superstructure causing excursions into 3D; b) the uniaxial clock model where consecutive layers in the three- and four-layer phases are rotated by 120° and 90°, respectively (plus a small angle due to the helix); and c) the model proposed by Lorman in which the intermediate phase structures are biaxial. In (c), a distortion angle is defined for each of the intermediate phases; here we define δ to be the smallest rotation angle in the three-layer case and half of the smallest angle in the four-layer phase.

disagreement about the terminology used for the three- and four-layer repeat phases. Only the three-layer phase is ferrielectric for all models and there is ambiguity for the four-layer structure. In this Minireview, we avoid confusion and refer to the phases simply by the number of layers in the repeat unit.

Levelut and Pansu^[16] predicted the positions and polarisations of the resonant peaks that would be observed in smectic liquid crystals, deriving the formula in Equation (1):

$$\frac{Q_z}{Q_0} = l + m \left(\frac{1}{\nu} \pm \varepsilon \right) \quad (1)$$

where Q_0 is the scattering vector of the Bragg peak, l is an integer that can take values of 0, ± 1 or ± 2 , ε is the ratio of the helicoidal pitch and the layer spacing and ν is the number of layers in the superlattice; for example, $\nu = 2$ for the SmC_A* (antiferroelectric) phase, 3 for the three-layer phase, etc. The resonant peaks should thus appear at various positions around the fundamental Bragg peaks, and it is clearly possible, in principle, to measure the helicoidal pitch from the separation of some of the peaks. The clock model and Lorman's model predict the first-order resonant peaks to be π -polarised, while the second-order peaks are σ -polarised for incident σ -polarised radiation.

The relative heights of the different peaks associated with a particular resonant reflection depend on the details of the structure and these can be calculated numerically by including the form factors for the structure. In the case of the symmetric clock model, the relative heights of the first-order peaks are predicted to be such that all the scattered intensity is in one of the two peaks ($+\epsilon$), so a single peak is observed. In the Lorman model, "distortion angles" feature (see Figure 3) which dictate the relative heights of the two possible first-order resonant peaks. The two models can thus be distinguished in principle, and the distortion angle can be calculated by numerically fitting the expected structures (calculated by including form factors for the structure) to experimental data. These predictions are summarised in Figure 3 and Table 1. It is clear that

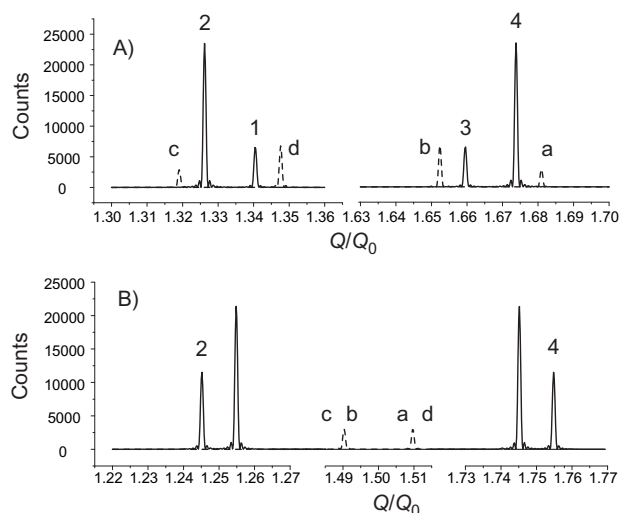


Figure 3. The positions and polarisation of the resonant peaks for A) the three- and B) the four-layer SmC* intermediate phases predicted for the structure suggested by Lorman^[20]. As discussed in the text, the details of the structure have a strong influence on the observation of these peaks; for example, if the three-layer structure is uniaxial, peaks labelled 1 and 3 would have zero height.

Table 1. The positions and polarisation states of the first- and second-order resonant peaks in the three- and four-layer structures for the Lorman model,^[20] deduced as an extension of the theory of Levelut and Pansu.^[16]

	l	m	Q/Q_0	Polarisation (σ incident)	Peak label (Figure 3)
three-layer first order	1	+1	$1 + 1/3 + \epsilon$	π	1
	1	+1	$1 + 1/3 - \epsilon$	π	2
	2	-1	$2 - 1/3 - \epsilon$	π	3
	2	-1	$2 - 1/3 + \epsilon$	π	4
three-layer second order	1	+2	$1 + 2/3 + 2\epsilon$	σ	a
	1	+2	$1 + 2/3 - 2\epsilon$	σ	b
	2	-2	$2 - 2/3 - 2\epsilon$	σ	c
	2	-2	$2 - 2/3 + 2\epsilon$	σ	d
four-layer first order	1	+1	$1 + 1/4 + \epsilon$	π	1
	1	+1	$1 + 1/4 - \epsilon$	π	2
	2	-1	$2 - 1/4 - \epsilon$	π	3
	2	-1	$2 - 1/4 + \epsilon$	π	4
four-layer second order	1	+2	$1 + 1/2 + 2\epsilon$	σ	a
	1	+2	$1 + 1/2 - 2\epsilon$	σ	b
	2	-2	$2 - 1/2 - 2\epsilon$	σ	c
	2	-2	$2 - 1/2 + 2\epsilon$	σ	d

resonant scattering can, in principle, determine unequivocally the structures of the SmC* subphases, though doing so in practice continues to provide a considerable challenge to experimentalists since the experiments are technically challenging.

Experimental Section

Resonant X-ray scattering experiments on liquid crystals require a synchrotron radiation source. The energy must be tuned with high accuracy to the absorption edge of a convenient atom, and high flux is necessary because the liquid crystal sample is usually very thin and the resonant peaks are weak. Two different geometries are appropriate for this kind of experiment. X-ray reflectivity measurements may be performed on free-standing smectic films, several microns in thickness. Alternatively, transmission experiments may be carried out by using liquid crystal devices in which the liquid crystal material is sandwiched between two thin glass plates. The two different experimental configurations are described in detail below.

Free-Standing Films: Free-standing films of smectic liquid crystals provide an excellent geometry for X-ray reflectivity measurements. Material is drawn slowly across an aperture forming a suspended liquid crystal film. Typically, films are spread in the orthogonal smectic A (SmA) phase, then cooled to the phase of interest for study. The smectic layers lie parallel to the substrate aperture and this geometry provides an excellent homeotropic alignment. The X-ray geometry for this experimental configuration can be seen in Figure 4a. As the liquid crystal film must be maintained in the smectic phase throughout the experiment, spreading is carried out in an enclosed oven system. The film thickness is estimated via optical observations of thin film interference.

A free-standing film geometry is preferred for phase characterisation as high-resolution resonant scattering and polarisation analysis may be achieved because of the excellent molecular alignment and signal-to-noise ratio. There are two disadvantages to this geometry. The experiments are carried out at grazing incidence (around 1°), so the beam footprint is significant, even when the beam dimensions are arranged to be a few tenths of a millimetre. The aperture for a free-standing film is consequently a few centimetres in width making spreading and temperature stability difficult.

It is also impossible to carry out switching studies in this geometry. Not only is the surrounding gas prone to ionisation by the high-energy X-rays, negating applied fields, but a typical film aperture of 10 mm in diameter would require an in-plane applied voltage of 10 000 V to observe ferroelectric switching at an applied electric field of $1 \text{ V } \mu\text{m}^{-1}$!

Liquid Crystal Devices: To carry out switching studies combined with resonant scattering, it is necessary to use a transmission geometry with a liquid crystal device specially constructed from thin ($170 \mu\text{m}$ thick) indium tin oxide (ITO) coated glass, Figure 4(b). The

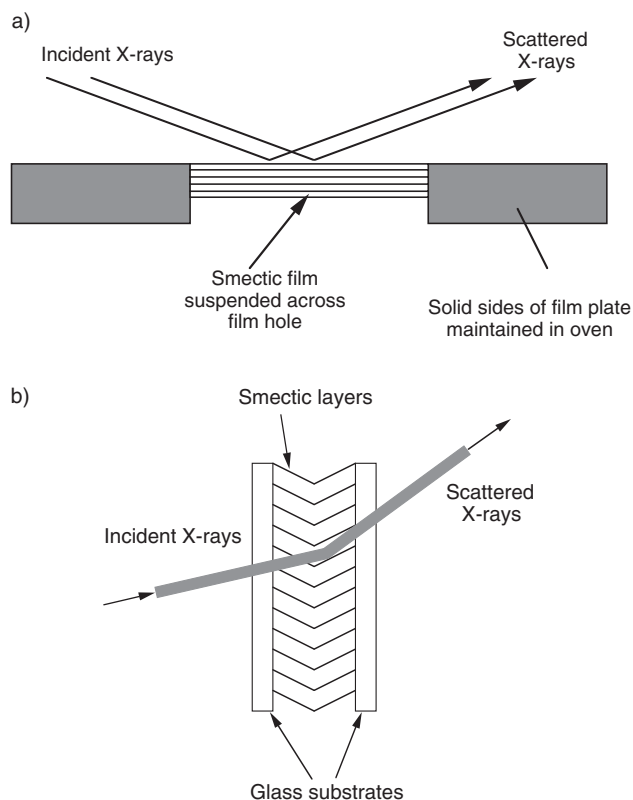


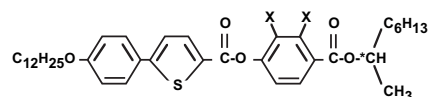
Figure 4. The scattering geometry usually used for a) a free-standing film sample and b) the side view of a typical device. The usual layer structure is shown in each case where lines represent the smectic planes. The layers are in the plane of the film in (a) and there would normally be several hundred layers in a film a few microns thick. In the device (b), the layers typically adopt the chevron structure shown with the layers at a small angle (the chevron angle—usually around $15\text{--}20^\circ$ in antiferroelectric liquid crystals) with respect to the plane of the glass. The liquid crystal film in the device is usually between $5\text{--}20\ \mu\text{m}$ in thickness. For typical antiferroelectric liquid crystals, the smectic layer spacing is around $35\ \text{\AA}$ so that the Bragg angle for $12.6\ \text{keV}$ X-rays is around $1\text{--}2^\circ$.

main concerns in such a transmission experiment are to minimise attenuation of the scattered X-rays from the device itself (hence, the use of thin glass), and to maximise the signal from the liquid crystal. The latter is achieved by producing an excellent liquid crystal monodomain within the device through coating the inner surfaces of the glass plates with a thin Nylon 6/6 alignment layer and rubbing with a soft cloth. This promotes uniform orientation of the liquid crystal director in the plane of the glass and the rubbing direction defines a symmetry axis. The glass plates are separated by a polyethyleneterephthalate spacer and enclose a $15\text{--}30\text{-}\mu\text{m}$ -thick liquid crystal sample. The ITO acts as an electrode, allowing the application of electric fields across the device. By using such techniques, it is easy to routinely apply electric fields up to $5\ \text{V}\ \mu\text{m}^{-1}$.

When material in a planar device is cooled into the SmA phase, the smectic layers will generally arrange themselves to lie perpendicular to the glass plates. This is known as the "bookshelf" geometry. On cooling further into a tilted phase, that is, the SmC* phase, the layers will typically remain anchored to the glass surfaces, therefore are forced to buckle to accommodate layer shrinkage. This is known as the "chevron" geometry.^[21] The angle of the chevron will vary with temperature and the associated change in layer

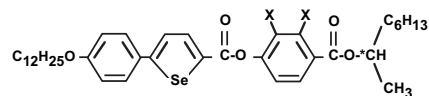
geometry within the device must be taken into account when aligning the device for X-ray measurements.

Materials: As discussed in the preceding sections, resonant scattering experiments are carried out by tuning the incident X-ray beam to scatter at the absorption edge energy of an atom in the liquid crystal molecule. Therefore, the technique requires a material with a suitable resonant atom, that is, one with a readily accessible absorption edge energy. Typical energies appropriate for scattering with synchrotron radiation are in the range $\approx 2\text{--}20\ \text{keV}$. Materials for the first resonant scattering experiments on liquid crystals were chosen to contain either sulphur^[15] (resonant energy $2.47\ \text{keV}$) or selenium^[22] (resonant energy $12.66\ \text{keV}$) in the rigid molecular core, as shown for compounds **A** and **B** in Figure 5. The positions of the resonant atom for each material can be seen in Figure 5 along with the phase sequence for each molecule. The materials are closely related in structure and each compound exhibits a rich phase sequence including some or all of the SmC* subphases. The structure–property relations of these materials have been reported elsewhere.^[23]



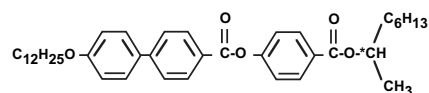
A1 K 64.2 SmC*_A 80.2 SmC*_{3-layer} 82.2 SmC* 92.6 SmA 97.9 I

A2 K 57.4 SmC*_A 64.0 SmC*_{3-layer} 65.0 SmC*_{4-layer} 68.6 SmC*_α 69.5 SmA 76.6 I



B1 K 67.7 SmC*_A 97.8 SmC*_{3-layer} 99.0 SmC* 109.4 SmA 116.6 I

B2 K 46.3 SmC*_A 79.7 SmC*_{3-layer} 83.3 SmC*_{4-layer} 84.3 SmC* 86.6 SmA 93.7 I



C K 72.9 SmC*_A 99.9 SmC*_{Fl} 103.5 SmC* 117.0 SmC*_a 122.2 SmA 129.3 I

Figure 5. The molecular structures and phase sequences of liquid crystal molecules typically used for resonant scattering experiments, as reported in ref. [29]. The resonant atoms are sulphur (compounds **A**) or selenium (compounds **B**) in the core of the molecules. Compounds **1** and **2** differ only in that both **A2** and **B2** are fluorinated on one of the aromatic rings in positions marked X, while **A1** and **B1** are unfluorinated. The fluorination has a remarkable effect on the phases observed in the system. Note that material **B1** exhibits hexatic ferroelectric and antiferroelectric phases on supercooling below the crystallisation temperature. The intermediate phase in compound **C** has not been identified as three- or four-layer; hence, it is marked as Fl.

Theoretically, any atom with an absorption edge in an accessible range can be used for these experiments. Bromine (Br) and Chlorine (Cl) are also potential candidates for this technique and materials containing both these atoms have been shown to give a resonant signal. Experiments with materials containing Br in the flexible tails of the molecule exhibited a lower signal-to-noise ratio than

those performed in systems where the resonant atom was contained in the molecular core.^[24] This is because the flexible tail is subject to much stronger fluctuations than the rigid core section, weakening the resonant scattering signal by effectively averaging the local environment. Nonetheless, resonant scattering was observed from the antiferroelectric phase. The first resonant scattering experiments on a liquid crystal at the chlorine K edge were carried out relatively recently on the B2 phase of bent-core liquid crystal compounds^[25], opening up a new class of compounds to the resonant scattering technique.

Experiments on selenium-containing materials were performed on beam lines 11D and 1BM at the Advanced Photon Source (APS) at Argonne National Laboratory. For materials containing sulphur, experiments were carried out at the National Synchrotron Light Source (NSLS) at Brookhaven National Laboratory on station X19A. Resonant scattering experiments have also been carried out on liquid crystals at the European Synchrotron Research Facility (ESRF).

Resonant Scattering from Free-Standing Films

Resonant scattering experiments have now been carried out on all the tilted smectic mesophases commonly observed in liquid crystal materials, and the key results are summarised below.

The SmC* Phase

Figure 6 shows a typical set of resonant scattering data from the SmC* phase. The (002) Bragg peak is shown along with the first- and second-order resonant peaks at the $m = \pm 1$ and $m = \pm 2$ positions, respectively. Away from the resonance condition, the (002) peak is still present but the resonant peaks are not. For all materials described here, this phase was present and the $m = \pm 1$ and $m = \pm 2$ resonant peaks were observed in free-standing films, though there is little interesting information to be deduced from measurements of these peaks. They confirm the theory and allow a direct measurement of the helicoidal pitch (from the separation of the peaks), though this measurement can often be more easily accessed by using other techniques.^[11,26]

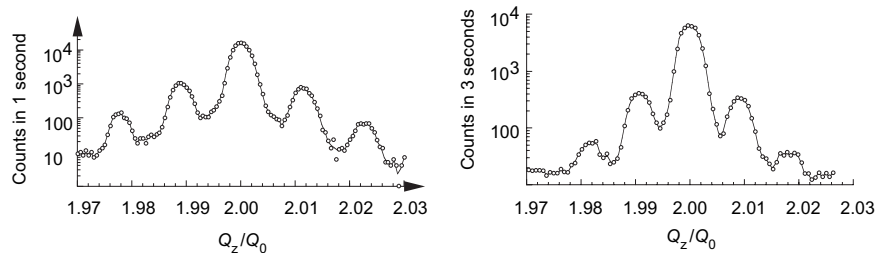


Figure 6. The resonant peaks observed around the 002 position in the SmC* phase of compounds **A1** (left) and **B1** (right), redrawn from ref. [29]. The separation of the satellites is dictated by the helicoidal pitch of the system in accordance with Equation (1).

The SmC*_A Phase

The SmC*_A phase has been well characterised in the past by conventional liquid crystal methods and the phase structure is well known.^[27] The first resonant scattering experiments were carried out on this phase and a structure of smectic layers with a molecular tilt alternating by approximately 180° about the switching cone from layer to layer was confirmed.^[28] Both first- and second-order resonant peaks have now been clearly observed^[29] and this phase is known to produce the clearest resonant signal of all the smectic phases. Figure 7 shows typical resonant scattering data in the antiferroelectric phase. The strong doublet at $Q_0/Q_z = 1.5 \pm \epsilon$ provides a nice measure of pitch in the material (ϵ is the ratio of the smectic layer spacing to the optical pitch).

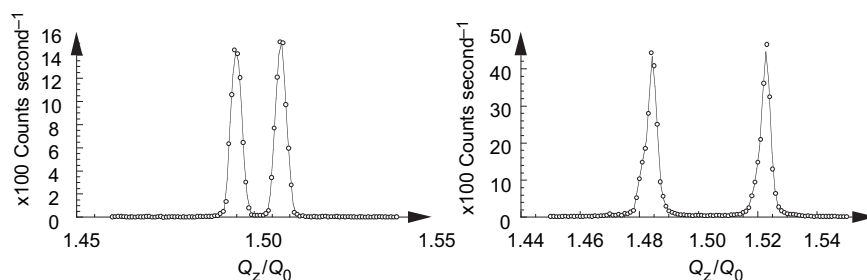


Figure 7. Resonant peaks around the 001.5 position in the antiferroelectric phases of compounds **B1** (left) and **B2** (right), redrawn from ref. [29]. The separation of the peaks is 2ϵ and it can be seen that in this case, the fluorination of the material has the effect of approximately halving the pitch.

The SmC*_α Phase

Resonant scattering has proved to be particularly useful in deducing the structure of the complicated SmC*_α phase. This phase occurs at higher temperatures than the SmC* phase and its structure is particularly interesting in the context of the current debate about the possible types of “De Vries” smectic phases.^[30] The first resonant scattering experiments on this phase observed first-order peaks and revealed a superlattice periodicity incommensurate with pitch, and which varies with temperature across the phase.^[28] Subsequently, resonant scattering from the SmC*_α phase was measured on several additional materials and more details were revealed in the second-order resonant features.^[29] The positions of these second-order

peaks were again consistent with the theoretical predictions of Levelut and Pansu.^[16] Figure 8 shows some typical data measured in the SmC*_α phase. It is interesting to note that the temperature-dependant superlattice periodicity in the SmC*_α phase varies significantly from material to material. A period of between five and eight layers was observed in compound **A2**, while in other materials, periodicities

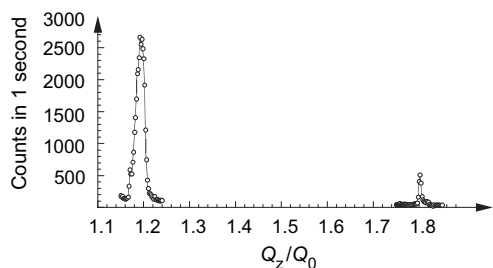


Figure 8. Resonant peaks for the alpha phase for material **A2** (redrawn from ref. [29]).

of ten layers and more were observed. In particular, the nature of the phase transitions between the SmA, SmC*_α, and SmC* phases is still not fully understood, although recent experiments have shown that the SmA–SmC*_α transition is continuous with XY-like critical exponents, while the SmC*_α–SmC* transition displays a rapid variation of the incommensurate helical pitch.^[31] More resonant scattering experiments in combination with careful optical measurements are required before this phase can be described in detail.

The Intermediate Phases

The first resonant scattering experiments^[28] revealed the periodicity of the highest-temperature intermediate phase to be four-layer and a polarisation analysis of the resonant peaks was used to distinguish between the two most likely theoretical models, the Ising model and the uniaxial clock model, shown in Figures 2a and 2b, respectively. The results indicated that the Ising model could be discounted. However, although these early resonant scattering data showed that the uniaxial clock model *could* be correct, evidence from optical methods such as ellipsometry^[32] and conoscopy^[33] revealed the phase to be locally biaxial about the layer normal. A biaxial model for the phase had been proposed by Lorman^[20] (Figure 2c) and it was predicted as an extension to the work of Levelut and Pansu that the first-order resonant peak would be split for a biaxial Lorman model. The degree of biaxiality (or distortion angle, δ) could then be calculated from the intensity ratio of the split peaks. A significant improvement in experimental resolution was achieved by the addition of a Ge analyser crystal before the detector and high-resolution (resolution of $4 \times 10^{-4} \text{ \AA}^{-1}$) resonant scattering was carried out, which confirmed the biaxial model and allowed the distortion angle to be measured.^[34] Simulations of the expected structure agreed very well with the observed data as can be seen in Figure 9 and a distortion angle of around $\delta = 18^\circ$ was deduced for several temperatures in the phase where helical pitch was not changing rapidly. As a result of these measurements, we now have an accurate description of the interlayer structure of the four-layer intermediate phase.

Experiments on the three-layer intermediate phase have always been difficult to undertake since the phase is typically stable only over $\approx 1^\circ\text{C}$, and it appears to be especially susceptible to beam damage during the resonant X-ray scattering experiments. A “forest” of peaks is often obtained, rather than

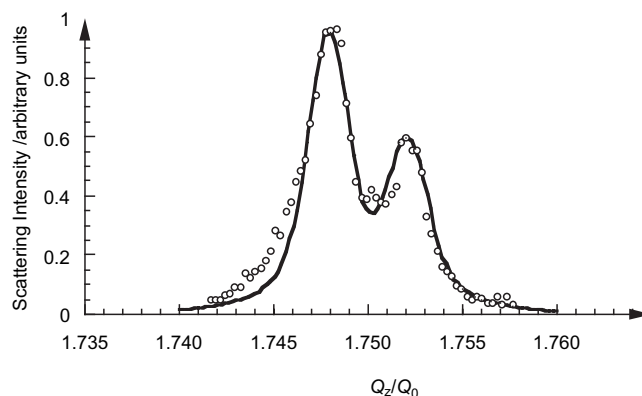


Figure 9. Split resonant peaks in the four-layer intermediate phase, allowing a deduction of the degree of biaxiality in the phase, redrawn from ref. [34]. The dark line shows a numerical fit to the data, giving a distortion angle of around 18° which was not found to be significantly temperature-dependant.

the well-defined resonant peaks characteristic of the other phases described here (see Figure 10 which shows data for compound **B2**). Very recently, new materials have been reported with remarkably wide three- and four-layer intermediate phases and high-resolution resonant scattering experiments on the three-layer phase are possible.^[35] Details of the structure of this phase, revealed by resonant scattering, have been reported very recently.^[36]

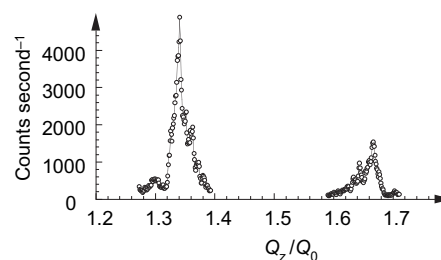


Figure 10. The “forest” of peaks around $Q_z/Q_0 = 1.33$ and 1.67 typical of the three-layer resonant signal.

Resonant Scattering from Liquid Crystal Mixtures

The resonant scattering technique is clearly a powerful diagnostic tool for phase characterisation when the liquid crystal molecule in question contains a suitable resonant atom. Relatively few liquid crystal molecules, however, contain such an atom with an easily accessible absorption edge energy. A more general approach involves doping a non-resonant liquid crystal material with a small amount of resonant material.^[29] Mixtures were made by combining compound **C** (non-resonant) with various proportions of compound **B1** (resonant) and it was shown that the addition of as little as 10% resonant material gave a strong signal in the antiferroelectric phase. Although it should be considered that the addition of liquid crystal dopants may affect the phase sequence of the material of interest,

particularly for the delicate SmC* subphases, the potential to go to even lower concentrations of resonant dopant is clear.

Resonant Scattering from Liquid Crystal Devices

The desirability of undertaking resonant scattering experiments on liquid crystal devices is clear. Most commercial studies and applications of liquid crystal properties and performance are carried out by using liquid crystal devices. Therefore, it is important to look at phase sequences and phase behaviour in that geometry. It is possible that certain phases may occur in a free-standing film geometry but are suppressed by the influence of the glass surfaces in a device geometry.^[37] Further, it is extremely easy to apply relatively high electric fields to a liquid crystal device and combine structural studies by resonant scattering with the switching properties of a material. All device-based experiments to date have been carried out on materials which contain selenium as the resonant atom.^[22,38] X-rays at the K absorption edge energy for sulphur (2.47 keV) are strongly attenuated by the glass plates of the liquid crystal device; however, such attenuation is minimal at the selenium K edge energy (12.66 keV).

Figure 11 A shows resonant peaks detected in the antiferroelectric phase for two different materials in a liquid crystal device. For a liquid crystal thickness of $\approx 20 \mu\text{m}$, the first-order resonant peaks are clearly observed with an excellent signal-to-noise ratio and the pitch can be deduced from the peak spacing. These data compare well with those obtained on free-standing films for the same materials, shown in Figure 7. Figure 11 B shows similar data but in the four-layer intermediate phase, confirming the existence of the four-layer phase in a device geometry. It is interesting to note that, to date, no resonant signature of the three-layer intermediate phase has been observed in a device geometry of any thickness.

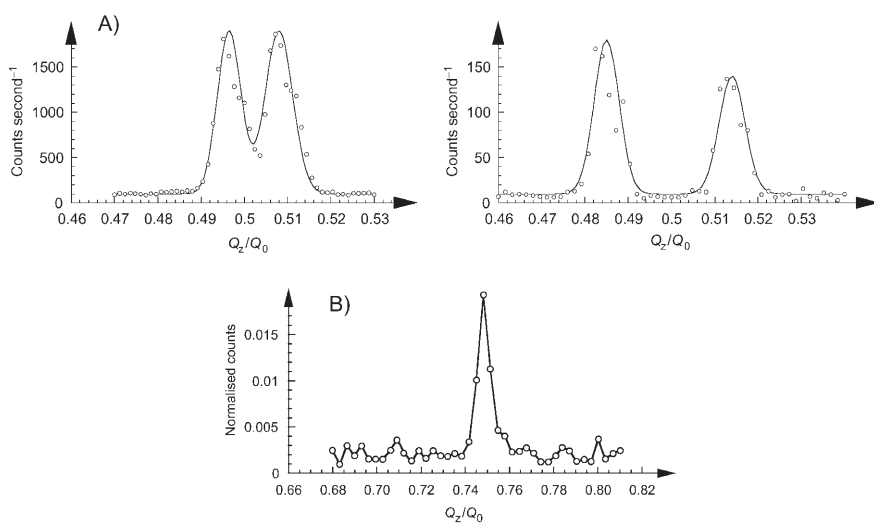


Figure 11. Data for A) the AFE phase, B) the four-layer phase within a conventional device geometry (redrawn from ref. [38]). The data in (A) are comparable to those shown in Figure 7.

Electric-Field Experiments

As already mentioned, the use of a specially constructed device allows resonant scattering experiments to be carried out while switching the system with electric fields, a geometry analogous to actual liquid crystal devices. This provides a powerful probe of the switching mechanisms in antiferroelectric devices, and offers a unique opportunity to study the influence of electric fields on the structure of the intermediate phases. The electric field is applied across the device, perpendicular to the smectic layer normal and data acquisition is triggered by the switching field such that scattering data are collected only during a specific part of the field cycle.

In the antiferroelectric phase, two different field-induced phenomena were investigated.^[29] Electric-field-induced unwinding of the helicoidal structure can occur at relatively low fields, lower than that necessary to induce a ferroelectric state. As already mentioned, resonant scattering is an excellent probe of the helicoidal pitch, so this is one phenomenon that is apparent from these experiments. Further, the onset of a field-induced ferroelectric state in a device with material in the antiferroelectric phase is apparent from the loss of the resonant scattering peaks at $Q_z/Q_0 = 0.5 \pm \epsilon$, $1.5 \pm \epsilon$, etc. Both field-dependant effects were investigated in compound **B1** by applying fields of successively higher magnitude to the device. It was noticed that the field at which point the antiferroelectric peaks disappeared was equivalent to that at which the smectic layers (initially in a chevron structure in the device) transformed to a bookshelf geometry.^[39,40] This experiment allowed us to confirm that the threshold field for ferroelectric switching in the antiferroelectric phase in compound **B1** is coincident with the chevron–bookshelf layer transformation.

A similar electric-field experiment was also performed on the SmC*_{4-layer} (intermediate) phase, a phase with a four-layer superlattice periodicity. Electric fields of gradually increasing amplitude were applied to the device and the interlayer molecular ordering monitored via the resonant peak at $Q_0/Q_z = 0.75 - \epsilon$. At an applied electric field of $0.71 \text{ V}\mu\text{m}^{-1}$, the device transformed into a bookshelf geometry but the four-layer ordering remained. Optical transmission experiments revealed distinct molecular rearrangements at 0.7 and $1.3 \text{ V}\mu\text{m}^{-1}$. By combining the conventional optical techniques used to study liquid crystal devices with resonant scattering we have been able to show that although the device shows some switching effects at very low electric fields the actual transition to ferroelectric switching does not occur until the relatively high field of $1.3 \text{ V}\mu\text{m}^{-1}$, higher than the chevron–bookshelf transition.

Conclusions

In this Minireview, we have summarised the major achievements of resonant X-ray scattering, a new technique for the characterisation of smectic liquid crystal mesophases. Over the past six years, this technique has been remarkably successful in the field of liquid crystals, providing a direct probe of the smectic phase structures. Utilising the position dependency of scattering from a resonant atom in the molecular core of a material, it has been possible to describe for the first time the structure of the smectic mesophases, in particular the controversial three- and four-layer intermediate phases and the alpha phase (SmC^*_α). This powerful technique has also been shown to work well in the study of liquid crystals held in a device geometry, such as is commonly used for liquid crystal phase study and applications. This then provides a unique probe of structure combined with electric-field application and switching studies.

There is considerable potential in the future for structural studies of other soft-matter systems. It should be noted that, so far, little is known about details of the three-layer phase though new mixtures are making it possible to carry out detailed studies of this phase, as well as probing the temperature dependence of this and the four-layer phase.^[36] It has already been shown that resonant scattering can be applied to materials at the chlorine K edge, including a study of the B2 phase of bent-core molecules. The newly discovered biaxial nematic systems are also formed from bent-core materials and contain intriguing smectic phases that have not yet been studied. In summary, new self-ordering materials are being discovered regularly. It is clear that very small changes in their molecular structure lead to subtle changes in packing that, in turn, can induce significant differences in bulk properties. The smectic phases described herein are an excellent example of that phenomenon and resonant X-ray scattering is an invaluable tool in deducing the subtleties of such structures.

Keywords: liquid crystals • smectic phases • structure elucidation • X-ray scattering

- [1] See, for example, *The Handbook of Liquid Crystals* (Ed.: D Demus, J Goodby), Wiley-VCH, Weinheim, **1998**.
- [2] P. S. Pershan, *Structure of Liquid Crystal Phases*, World Scientific, Singapore, **1988**.
- [3] S. Kumar, *Liquid Crystals, Experimental Study of Physical Properties and Phase Transitions* (Ed.: S Kumar), Cambridge University Press, Cambridge, **2001**.
- [4] P. S. Clegg, *Acta Crystallogr. Sect. A* **2005**, *61*, 112.
- [5] D. H. Templeton, L. K. Templeton, *Acta Crystallogr. Sect. A* **1980**, *36*, 237.
- [6] V. E. Dmitrienko, *Acta Crystallogr. Sect. A* **1983**, *39*, 29.
- [7] V. E. Dmitrienko, *Acta Crystallogr. Sect. A* **1984**, *40*, 89.
- [8] D. H. Templeton, L. K. Templeton, *Acta Crystallogr. Sect. A* **1985**, *41*, 133; D. H. Templeton, L. K. Templeton, *Acta Crystallogr. Sect. A* **1985**, *41*, 365.
- [9] P. J. Collings, M. Hird, *Introduction to Liquid Crystals*, Taylor and Francis, London, **1997**.
- [10] R. B. Meyer, L. Lieberh, L. Strzelecki, P. Keller, *J. Phys.* **1975**, *36*, 69.
- [11] *Ferroelectric liquid crystals, Principles, Properties and Applications* (Ed.: Goodby et al.), Gordon and Breach, Amsterdam, **1991**.
- [12] A. D. L. Chandani, E. Goreka, Y. Ouchi, H. Takezoe, A. Fukuda, *Jpn. J. Appl. Phys. Part 1* **1989**, *28*, L1265.
- [13] M. Fuki, H. Orihara, Y. Yamada, N. Yamamoto, Y. Ishibashi, *Jpn. J. Appl. Phys. Part 1* **1989**, *28*, L849.
- [14] A. D. L. Chandani, Y. Ouchi, H. Takezoe, A. Fukuda, K. Tersshima, K. Furukawa, A. Hishi, *Jpn. J. Appl. Phys. Part 1* **1989**, *28*, L1261.
- [15] P. Mach, R. Pindak, A.-M. Levelut, P. Barois, H. T. Nguyen, C. C. Huang, L. Furenliid, *Phys. Rev. Lett.* **1998**, *81*, 1015.
- [16] A.-M. Levelut, B. Pansu, *Phys. Rev. E* **1999**, *60*, 6803.
- [17] M. Cepic, B. Zeks, *Mol. Cryst. Liq. Cryst.* **1995**, *263*, 61.
- [18] S. A. Pikin, *Mol. Cryst. Liq. Cryst.* **1995**, *262*, 425.
- [19] A. Roy, N. V. Madhusudana, *Europhys. Lett.* **1996**, *36*, 221.
- [20] V. L. Lorman, *Liq. Cryst.* **1996**, *20*, 267.
- [21] T. P. Reiker, N. A. Clark, G. S. Smith, D. S. Parmar, E. B. Sirota, C. R. Safinya, *Phys. Rev. Lett.* **1987**, *59*, 2658.
- [22] L. S. Matkin, H. F. Gleeson, P. Mach, C. C. Huang, R. Pindak, G. Srajer, J. Pollmann, J. W. Goodby, M. Hird, A. Seed, *Appl. Phys. Lett.* **2000**, *76*, 1863.
- [23] J. T. Mills, R. J. Miller, H. F. Gleeson, A. J. Seed, M. Hird, P. Styring, *Mol. Cryst. Liq. Cryst.* **1997**, *303*, 145.
- [24] P. Cluzeau, P. Gisse, V. Ravaine, A. M. Levelut, P. Barois, C. C. Huang, F. Rieutord, H. T. Nguyen, *Ferroelectrics* **2000**, *244*, 301.
- [25] A. Cady, R. Pindak, W. Caliebe, P. Barois, W. Weissflog, H. T. Nguyen, C. C. Huang, *Liq. Cryst.* **2002**, *29*, 1101.
- [26] N. W. Roberts, H. F. Gleeson, N. Bowring, A. Seed, J. W. Goodby, M. Hird, *J. Mater. Chem.* **2003**, *13*, 353.
- [27] *The Physics of Ferroelectric and Antiferroelectric liquid crystals* (Ed.: I. Muševic, R. Blinc, B. Zeks), World Scientific, Singapore, **2000**.
- [28] P. Mach, R. Pindak, A. M. Levelut, P. Barois, H. T. Nguyen, H. Baltes, M. Hird, K. Toyne, A. Seed, J. W. Goodby, C. C. Huang, L. Furenliid, *Phys. Rev. E* **1999**, *60*, 6793.
- [29] L. S. Hirst, S. J. Watson, H. F. Gleeson, P. Cluzeau, R. Pindak, J. Pitney, A. Cady, P. Johnson, C. C. Huang, A.-M. Levelut, P. Barois, G. Srajer, J. Pollmann, W. Caliebe, A. Seed, M. R. Herbert, J. W. Goodby, M. Hird, *Phys. Rev. E* **2002**, *65*, 041705.
- [30] See A. de Vries, *J. Chem. Phys.* **1979**, *71*, 25; A. de Vries, *Mol. Cryst. Liq. Cryst.* **1979**, *49*, 179.
- [31] C. C. Huang, Z. Q. Liu, A. Cady, R. Pindak, W. Caliebe, P. Barois, H. T. Nguyen, K. Ema, K. Takekoshi, H. Yao, *Liq. Cryst.* **2004**, *31*, 127.
- [32] P. M. Johnson, D. A. Olson, S. Pankratz, T. Nguyen, J. Goodby, M. Hird, C. C. Huang, *Phys. Rev. Lett.* **2000**, *84*, 4870.
- [33] L. Baylis, J. T. Mills, H. F. Gleeson, M. Hird, P. Styring, A. Seed, J. W. Goodby, *Mol. Cryst. Liq. Cryst.* **1999**, *328*, 13.
- [34] A. Cady, J. A. Pitney, R. Pindak, L. S. Matkin, S. J. Watson, H. F. Gleeson, P. Cluzeau, P. Barois, A.-M. Levelut, W. Caliebe, J. W. Goodby, M. Hird, C. C. Huang, *Phys. Rev. E* **2001**, *64*, 050702(R).
- [35] H. F. Gleeson, R. Pindak, W. Wang, N. Roberts, Z. Liu, S. Jaradat, J. Bai, Poster PO43, *20th International Liquid Crystal Conference*, Slovenia, **2004**.
- [36] N. W. Roberts, S. Jaradat, L. S. Hirst, M. S. Thurlow, Y. Wang, S. T. Wang, Z. Q. Lui, C. C. Huang, J. Bai, R. Pindak, H. F. Gleeson, *Europhys. Lett.* **2005**, *72* (6), 976–982.
- [37] See, for example, J. P. F. Lagerwall, D. D. Parghi, D. Kruerke, F. Gouda, P. Jagemalm, *Liq. Cryst.* **2002**, *29*, 163.
- [38] L. S. Matkin, H. F. Gleeson, S. J. Watson, R. Pindak, J. Pitney, P. M. Johnson, C. C. Huang, P. Barois, A.-M. Levelut, G. Srajer, J. Pollmann, J. W. Goodby, M. Hird, *Phys. Rev. E* **2001**, *64*, 021705.
- [39] L. S. Matkin, H. F. Gleeson, S. Watson, L. Baylis, N. Bowring, J. W. Goodby, M. Hird, A. Seed, *Appl. Phys. Lett.* **2000**, *77*, 340–342.
- [40] S. Watson, H. F. Gleeson, L. Matkin, L. Baylis, N. Bowring, M. Hird, J. Goodby, *Phys. Rev. E* **2002**, *65*, 031705.

Received: July 29, 2005